Observation of Reduced Electron-Temperature Fluctuations in the Core of H-Mode Plasmas

L. Schmitz,[1] A. E. White,[1] T. A. Carter,[1] W. A. Peebles,[1] T. L. Rhodes,[1] K. H. Burrell,[2] W. Solomon,[3] and G. M. Staebler[2]

[1]*Department of Physics and Astronomy, University of California, Los Angeles, Los Angeles, California 90024-2704, USA*

[2]*General Atomics, San Diego, California 92186-5608, USA*

[3]*Princeton Plasma Physics Laboratory, Princeton, New Jersey 08543-0451, USA*

(Received 9 October 2007; published 23 January 2008)

Core electron-temperature fluctuations [$0.5\% \leq \tilde{T}_e/T_e \leq 2\%$, $k_\theta \rho_s \leq 0.3$ in neutral-beam-heated low confinement-mode (L-mode) plasmas] are observed to decrease by at least a factor of 4 in standard and quiescent high-confinement-mode (H-mode and QH-mode) regimes in the DIII-D tokamak ($r/a = 0.7$). These fluctuations are attributed to ion temperature gradient (ITG) modes stabilized by rotational shear at the H-mode transition. The simultaneous reduction in electron heat diffusivity ($\chi_e^{\mathrm{QH}}/\chi_e^{L} < 0.25$) suggests that $\tilde{T}_e$ fluctuations can contribute significantly to L-mode electron heat transport.

DOI: 10.1103/PhysRevLett.100.035002 PACS numbers: 52.55.Fa, 52.25.Fi, 52.35.Ra, 52.70.Gw

Electron heat transport is a critically important process in magnetized plasmas. For example, the study of astrophysical plasmas [1], laser-produced plasmas [2], and high temperature fusion plasmas [3] all benefit from improved understanding of the underlying physical mechanisms. Anomalous transport perpendicular to the confining magnetic field presents a considerable challenge for magnetic fusion research [3,4]. The high transport rate (compared to the expected rate due to classical/neoclassical collisional processes) is thought to result from plasma turbulence, although many critical issues remain unresolved. The anomalous electron heat flux driven by electrostatic fluctuations can be expressed as [5]:

$$Q_e^{\mathrm{fl}} = \tfrac{3}{2}(nk_B T_e)/B_t(\langle(\tilde{T}_e/T_e)\tilde{E}_\theta\rangle + \langle(\tilde{n}/n)\tilde{E}_\theta\rangle). \quad (1)$$

Here, n, T_e, and B_t are the density, electron temperature, and toroidal magnetic field, respectively, and $\tilde{T}_e$, $\tilde{E}_\theta$, and $\tilde{n}$ are the electron temperature, poloidal electric field, and density fluctuation levels. The brackets denote a time average. As can be seen from the symmetry of Eq. (1), electron-temperature fluctuations and density fluctuations have the potential to contribute equally to the anomalous heat flux. However, turbulence studies in the core of high-performance fusion plasmas have focused primarily on density fluctuations, which are accessible by a variety of diagnostic techniques. In contrast, the role of core electron-temperature fluctuations to the improved confinement observed after transition from low confinement (L-mode) to high confinement (H-mode) plasmas has not been previously investigated. H-mode and quiescent H-mode (QH-mode) plasmas [6–9] in the DIII-D tokamak (major radius $R = 1.67$ m, minor radius $a = 0.61$ m, toroidal magnetic field $B_t = 2.1$T) are characterized by reduced cross-field particle, ion thermal, and electron thermal transport. Previously, density fluctuations have been observed to decrease at the L-mode to H-mode transition [10]. These reductions have been invoked as an explanation of the reduced particle and ion heat transport found in H mode.

The measurements reported here establish that relative temperature fluctuation levels are similar in magnitude to density fluctuations during L-mode operation, and, more importantly, are observed to reduce by at least a factor of 4 and 5, respectively, in the core of H-mode and quiescent H-mode (QH) regimes. This fundamental new information on turbulence reduction in H-mode plasmas strongly suggests that electron-temperature fluctuations contribute significantly to the observed decrease in anomalous (turbulent-driven) electron heat flux.

Electron cyclotron emission (ECE) is routinely used in tokamak plasmas to determine the electron-temperature profile since the magnetic field varies spatially and a particular emission frequency corresponds to one spatial location in the plasma [11]. In a conventional single-sideband heterodyne radiometer the minimum detectable fluctuation level of the radiation temperature, $\tilde{T}_{R,\mathrm{min}}/T_R$, is determined by the ratio of the intermediate frequency (IF) bandwidth B_{IF} and the postdetection bandwidth B_v [12], $\tilde{T}_{R,\mathrm{min}}/T_R = (B_v/B_{\mathrm{IF}})^{1/2}$. For the receiver system employed here ($B_{\mathrm{IF}} \sim 100$ MHz, $B_v \sim 0.5$ MHz), $\tilde{T}_{R,\mathrm{min}}/T_R = 7\%$. The actual temperature fluctuation level reported here is much lower; therefore a cross-correlation technique (CECE) is required to extract temperature fluctuations from the ECE signal. CECE measurements have previously been carried out in Ohmic [13–15], electron-cyclotron-resonance-heated (ECRH) [16,17] and rf-heated [15] fusion plasmas. The CECE method employed here cross-correlates signals from two closely spaced frequency intervals. Electron-temperature fluctuations related to plasma turbulence remain correlated if the probed emission volumes lie within the radial correlation length of the temperature fluctuations. In contrast, inherent fluctuations in the ECE signal, related to thermal emission, are decorrelated provided the frequency intervals do not overlap.

We employ a heterodyne correlation radiometer with both channels receiving 2nd harmonic X-mode cyclotron emission along the same line of sight [13–15]. The experi-

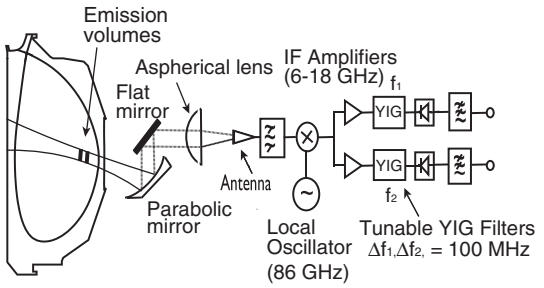

FIG. 1. Schematic of the experimental arrangement.

mental arrangement used on DIII-D is shown schematically in Fig. 1. A parabolic mirror located inside the vacuum collects radiation from the plasma at an angle of 7° to the tokamak midplane. The measured beam diameter at the $1/e$ power points is $D \sim 2.5$ cm for normalized radii $0.5 < r/a < 0.8$, where r is the emission radius and a is the plasma boundary radius.

Hence the diagnostic is most sensitive to fluctuations with a poloidal wave number $k_{\theta\,\mathrm{max}} \leq \pi/D = 1.3\ \mathrm{cm}^{-1}$. The frequency band 92–106 GHz is down-converted to the 6–18 GHz frequency range. Two tunable yttrium-iron garnet (YIG) bandpass filters ($B_{\mathrm{IF}} = 100$ MHz corresponding to a radial resolution $\Delta r \sim 0.3$ cm) are used to discriminate the radiation emitted from adjacent plasma volumes.

The relative radiation temperature fluctuation amplitude is given by the correlation coefficient of the CECE signals $C_{12}(\Delta t)$ [18], according to $\tilde{T}_R/T_R = [C_{12}(\Delta t = 0)]^{1/2} \times (B_v/B_{\mathrm{IF}})^{1/2}$. For the typical sample record length $\Delta T = 0.2$ s used in this experiment a detection limit of 0.33% is determined from the variance $\varepsilon^2[C_{12}(0)] = (B_v/B_{\mathrm{IF}})/(2B_v\Delta T)^{1/2}$ [18]. The optical depth at the measurement location ($r/a = 0.7$) is $\tau \geq 4$ [19]. Including the effect [16] of density fluctuations [$\tilde{n}/n \leq 0.02$ for $r/a = 0.7$ from beam emission spectroscopy (BES) [20]] requires a maximum correction of less than 10% in order to interpret the measurement as true electron-temperature fluctuations.

CECE measurements have been performed in upper single null, beam-heated discharges in the L-mode, H-mode, and QH-mode regimes (Fig. 2). Neutral-beam power (2.6 MW) is counterinjected at 400 ms followed by the addition of a second 2.1 MW counter-beam source at 800 ms. This leads to the H-mode transition at $t = 900$ ms as indicated by the sudden drop in the midplane deuterium D_α emission intensity [Fig. 2(d)]. During H mode, the line-averaged density increases threefold (due to improved particle confinement). The central electron and ion temperatures increase from 1.5 to 3.8 keV, and from 1.5 to 12 keV, respectively, and the global energy confinement time increases by a factor of 2.5–3 after the H-mode transition and during the QH-mode phase. QH-mode plasmas are characterized by the absence of edge-localized modes (ELMs), which, in a regular H mode, typically occur a few hundred ms after the L- to H-mode transition.

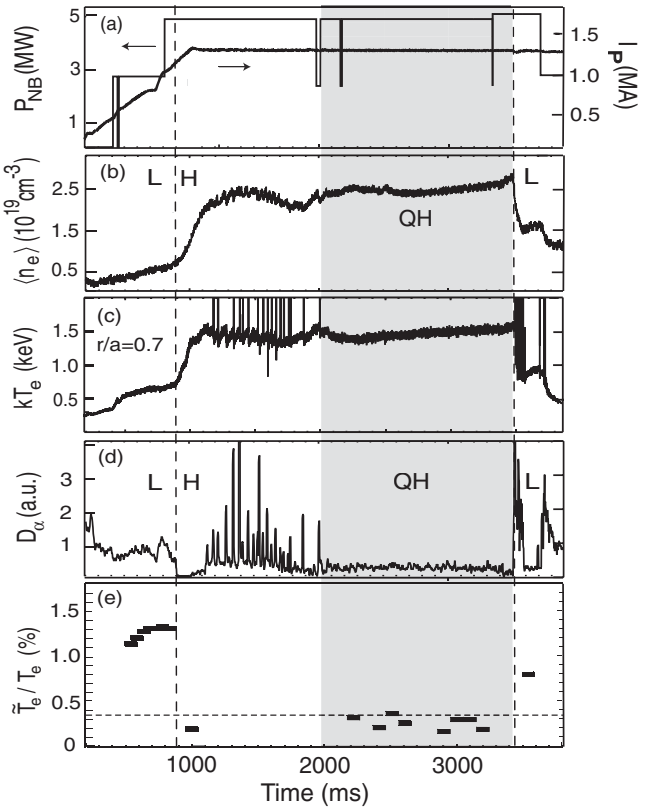

FIG. 2. (a) Injected neutral-beam power and plasma current; (b) line-averaged density; (c) electron temperature at $r/a = 0.7$; (d) D_α line emission intensity; (e) normalized electron-temperature fluctuation level for shot no. 125113. L-H and H-L transitions are indicated by vertical dashed lines, the QH-mode phase is shaded.

During the L-mode phase the relative temperature fluctuation level at $r/a \sim 0.7$ rises to $\tilde{T}_e/T_e \sim 1.3\%$. After the transition to H mode the fluctuation level drops by at least a factor of 4 to a value at or below the minimum detectable level of 0.33% [Fig. 2(e), using a 0.2 s record length]. The fluctuation amplitude does not rise above this level during the entire QH-mode phase (2000–3500 ms). Reducing the detection limit to 0.24% by using a record length of 800 ms, the QH-mode *relative* temperature fluctuation level was found to be more than a factor of 5 below that observed during the preceding L-mode phase ($r/a = 0.7$). Although the electron temperature during QH mode has increased by a factor of 2.5, the *absolute* electron-temperature fluctuation level $\tilde{T}_e$ has reduced by a factor of approximately 2 compared to L mode. Edge harmonic oscillations (EHO modes) present during the QH-mode phase at $r/a > 0.85$ do not affect the CECE measurements at $r/a = 0.7$.

Figure 3 shows the measured correlation coefficient $C_{12}(\Delta t)$ of the ECE signals and the fluctuation cross-power spectra $P_{12}(f) = [\tilde{T}_R(f)/T_R]^2$ during the L mode with 2.4 MW (a),(b) and 4.7 MW (c),(d) beam injection power and during ELM-free H mode of DIII-D discharge

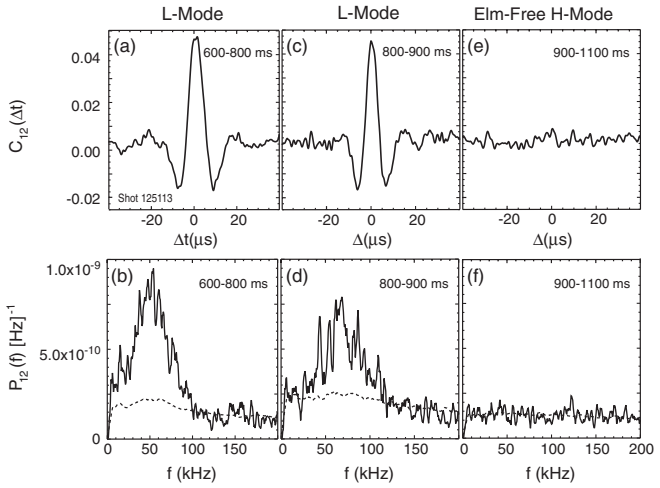

FIG. 3. Correlation coefficient and cross-power spectra before and after the H-mode transition ($t_{\text{L-H}} = 900$ ms). The data are integrated over 200 ms (a)–(b), (e)–(f), and 100 ms (c)–(d).

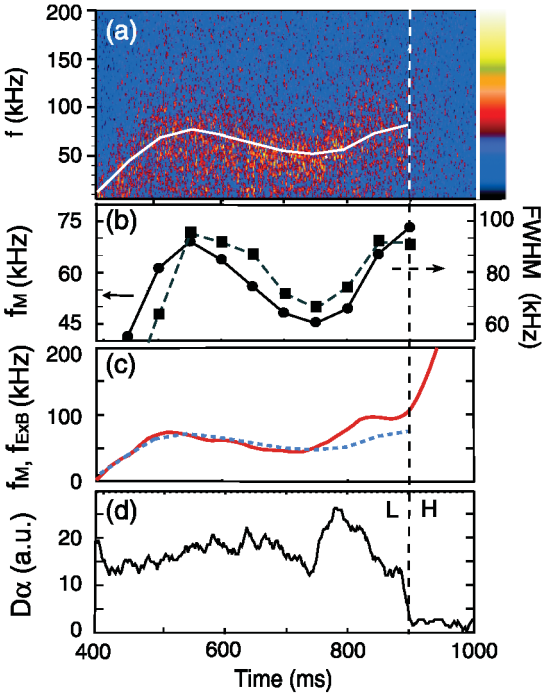

FIG. 4 (color). (a) Cross-power spectrum $P_{12}(f, t) = [\tilde{T}_R(f, t)/T_R(t)]^2$ and mean frequency f_M (white line); the vertical dashed line indicates the L-H transition; (b) mean frequency f_M and frequency FWHM of spectrum in (a); (c) $\boldsymbol{E} \times \boldsymbol{B}$ frequency $f_{\boldsymbol{E}\times\boldsymbol{B}} = v_{\boldsymbol{E}\times\boldsymbol{B}}(r/a = 0.7)k_\theta/2\pi$ for $k_\theta = 1.25$ cm^{-1}, and f_M (dashed line); (d) D_α line intensity indicating the timing of the L-H transition.

no. 125113. Broadband temperature fluctuations (5 kHz $< f <$ 150 kHz) are observed during L mode, while in H mode both the correlation coefficient and the spectral intensity are near the statistical detection limit (dashed lines).

The temporal evolution of the cross-power spectrum with 25 ms time resolution is shown in Fig. 4(a). The mean frequency and width [Fig. 4(b)] of the spectral feature are observed to evolve in response to changes in beam-driven plasma rotation which dominate the dispersive properties, i.e., the $\boldsymbol{E} \times \boldsymbol{B}$ plasma flow far exceeds the phase velocity of the fluctuations. The poloidal wave number detected by the CECE diagnostic can therefore be independently estimated from the spectral mean frequency according to $k_\theta \sim 2\pi f_M/v_{\boldsymbol{E}\times\boldsymbol{B}}$. Figure 4(c) shows that the measured mean frequency of the temperature fluctuation spectrum follows almost exactly the $\boldsymbol{E} \times \boldsymbol{B}$ rotation frequency, $f_{\boldsymbol{E}\times\boldsymbol{B}} = v_{\boldsymbol{E}\times\boldsymbol{B}}(r/a = 0.7)k_\theta/2\pi$ determined from charge exchange recombination (CER) measurements [21], using $k_\theta = 1.25$ cm^{-1} ($k_\theta\rho_s \sim 0.25$). Suppression of fluctuations is clearly observed close to the time of the L-H transition [$t = 900$ ms, Fig. 4(a)]. The expected broadening and shift of the temperature fluctuation spectrum lie well within the signal bandwidth ($\Delta f \sim 0.5$ MHz) and cannot explain the observed fluctuation reduction.

For typical tokamak plasma parameters, turbulence can be driven by the ion temperature gradient (ITG modes) [22], the electron-temperature gradient (ETG modes) [23], or by the trapped electron population (TEM modes) [24], depending on the detailed local gradients, collisionality, and magnetic shear. The diagnostic used here is most sensitive to ITG/TEM turbulence with low and/or medium poloidal wave numbers ($k_\theta\rho_s \leq 0.25$ in L mode and $k_\theta\rho_s \leq 0.5$ in H and QH mode), while short wavelength ETG modes ($k_\theta\rho_s > 3$) cannot be observed.

Linear stability calculations with the three-dimensional trapped gyro landau fluid (TGLF) code [25,26] indicate that the ITG mode is the dominant instability for $0.1 \leq k_\theta\rho_s \leq 1$ during the L-mode phase of the discharge at the measurement radius ($r/a = 0.7$), with TEM growth rates $\gamma_{\text{TEM}} < 0.2\gamma_{\text{ITG}}$. These results suggest that the observed electron-temperature fluctuations are associated with the ITG mode, possibly resulting from a nonadiabatic electron response. The maximum linear growth rate ($\gamma_L \sim 5 \times 10^4$ s^{-1}) is found at $k_\theta\rho_s \sim 0.6$. The experimentally inferred mean poloidal wave number $k_\theta \sim 1.25$ cm^{-1} [$k_\theta\rho_s \sim 0.25$, Fig. 4(c)] for the observed temperature fluctuations lies well within the linearly unstable ITG wave number range. Figure 5 shows results of transport analysis carried out using the ONETWO code [27]. The electron heat diffusivity ($\chi_e \sim 1.5 \times 10^5$ cm^2/s in L mode at the measurement location, $r/a = 0.7$) is found to be greatly reduced in H and QH mode for $r/a > 0.4$. For $r/a = 0.7$, $\chi_e^{\text{QH}}/\chi_e{}^L \sim 0.22$.

Figure 5 also shows the ratio of the $\boldsymbol{E} \times \boldsymbol{B}$ shearing rate to the linear growth rate at $r/a = 0.7$. In L mode, the linear ITG growth rate far exceeds the flux-surface-averaged shearing rate $\omega_{ExB} = \langle[(RB_\theta)^2/B_t](\partial/\partial\psi)(E_r/RB_\theta)\rangle$ due to $\boldsymbol{E} \times \boldsymbol{B}$ plasma rotation [28]. Here, B_θ is the poloidal magnetic field, and E_r is the radial electric field. Hence, in

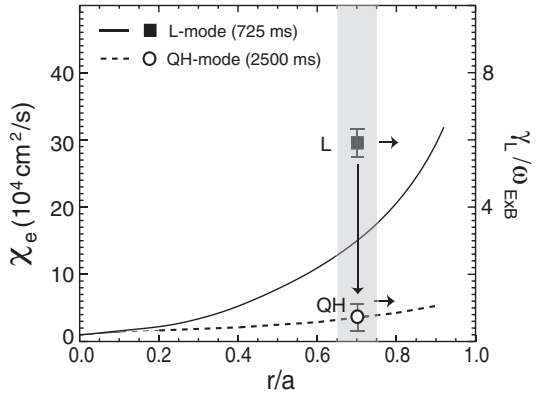

FIG. 5. Electron heat diffusivity in L mode (solid line) and QH mode (dashed line). Also shown is the ratio of the linear growth rate γ_L (calculated with the TGLF code for $k_\theta = 1.25$ cm^{-1}) to the $\boldsymbol{E} \times \boldsymbol{B}$ shearing rate $\omega_{\boldsymbol{E}\times\boldsymbol{B}}$.

L mode, flow shear stabilization is not expected to suppress ITG modes. In H and QH mode, TEM modes are found to dominate in the linear stability analysis. However, here the $\boldsymbol{E} \times \boldsymbol{B}$ shearing rate is found to exceed the calculated linear growth rate, in agreement with previous results invoking sheared $\boldsymbol{E} \times \boldsymbol{B}$ rotation to explain stability of long wavelength microturbulence in H mode [29].

The relative temperature fluctuation levels in L mode, $\tilde{T}_e/T_e \leq 2\%$, are similar to the L-mode density fluctuation levels $\tilde{n}/n$ measured in DIII-D by beam emission spectroscopy ($k_\theta \leq 3$ cm^{-1}) [20]. The observed dramatic reduction in electron-temperature fluctuation level during H mode correlates with the reduced electron heat diffusivity and the reduction of the density fluctuation level typically observed from reflectometry and BES [20]. In view of the symmetry of the anomalous electron heat flux Q_e^{fl} with regard to density and temperature fluctuations [Eq. (1)], these findings indicate that electron-temperature fluctuations substantially contribute to or possibly dominate anomalous core electron heat flux in L mode.

In conclusion, we have presented the first experimental observation of a large reduction in core plasma electron-temperature fluctuations at the transition from L mode to H mode and during QH mode. The association of electron-temperature fluctuations with the ITG-mode regime (as suggested here by linear stability analysis) has not been studied extensively either experimentally or in nonlinear gyrokinetic simulations to date, and may be indicative of a nonadiabatic electron response due to the trapped electron population. This suggests that correlated electron-temperature and poloidal-electric-field fluctuations [Eq. (1)] can play an important role in L-mode electron heat transport. A direct comparison of measured temperature fluctuation levels and spectra with nonlinear gyrokinetic simulation results may help to more conclusively elucidate the mechanisms responsible for anomalous electron heat transport. Simultaneous measurements of correlated electron-temperature and density fluctuations are planned for DIII-D, using reflectometry and CECE data obtained at the same spatial location. This will allow their phase relationship to be determined which will shed further light on the nature of turbulence-driven electron heat transport in magnetic confinement fusion plasmas.

This work is supported by the U.S. Department of Energy under Contracts No. DE-FG03-01ER54615, No. DE-AC02-76CH03073, and No. DE-FC02-04ER54698, and General Atomics Subcontract No. NS53250.

[1] B. D. G. Chadran and J. L. Maron, Astrophys. J. **602**, 170 (2004).
[2] M. Strauss *et al.*, Phys. Rev. A **30**, 2627 (1984).
[3] B. A. Carreras, IEEE Trans. Plasma Sci. **25**, 1281 (1997).
[4] A. J. Wootton *et al.*, Phys. Fluids B **2**, 2879 (1990).
[5] D. W. Ross, Plasma Phys. Controlled Fusion **34**, 137 (1992).
[6] F. Wagner *et al.*, Phys. Rev. Lett. **49**, 1408 (1982).
[7] R. J. Groebner, K. H. Burrell, and R. P. Seraydarian, Phys. Rev. Lett. **64**, 3015 (1990).
[8] K. H. Burrell *et al.*, Plasma Phys. Controlled Fusion **46**, A165 (2004).
[9] K. H. Burrell *et al.*, Phys. Plasmas **12**, 056121 (2005).
[10] C. L. Rettig *et al.*, Nucl. Fusion **33**, 643 (1993).
[11] A. E. Costley *et al.*, Phys. Rev. Lett. **33**, 758 (1974).
[12] G. Bekefi, *Radiation Processes in Plasmas* (Wiley, New York, 1966).
[13] G. Cima *et al.*, Phys. Plasmas **2**, 720 (1995).
[14] V. S. Udintsev *et al.*, Fusion Sci. Technol. **50**, 508 (2006).
[15] C. Watts *et al.*, Nucl. Fusion **44**, 987 (2004).
[16] S. Sattler *et al.*, Phys. Rev. Lett. **72**, 653 (1994).
[17] B. H. Deng *et al.*, Phys. Plasmas **8**, 2163 (2001).
[18] J. S. Bendat and A. G. Piersol, *Random Data: Analysis and Measurement Procedures* (Wiley, New York, 1986).
[19] M. Bornatici *et al.*, Plasma Phys. **23**, 1127 (1981).
[20] G. R. McKee *et al.*, Plasma Fusion Res. **2**, S1025 (2007).
[21] W. M. Solomon *et al.*, Phys. Plasmas **13**, 056116 (2006).
[22] W. Horton, Rev. Mod. Phys. **71**, 735 (1999).
[23] W. Horton *et al.*, Phys. Fluids **31**, 2971 (1988).
[24] J. Weiland *et al.*, Nucl. Fusion **29**, 1810 (1989).
[25] G. M. Staebler, J. E. Kinsey, and R. E. Waltz, Phys. Plasmas **12**, 102508 (2005).
[26] G. M. Staebler, J. E. Kinsey, and R. E. Waltz, Phys. Plasmas **14**, 055909 (2007).
[27] H. St. John *et al.*, Plasma Phys. Controlled Nucl. Fusion Res. **3**, 603 (1994).
[28] K. H. Burrell, Phys. Plasmas **4**, 1499 (1997).
[29] D. R. Baker *et al.*, Phys. Plasmas **10**, 4419 (2003).